

MODELLING THE EFFECT OF RESIDUAL STRESSES ON DAMAGE ACCUMULATION USING A COUPLED CRYSTAL PLASTICITY PHASE FIELD FRACTURE APPROACH

Michael Salvini^{1,†,*}, Nicolò Grilli^{1†,*}, David Knowles^{2,1}, Mahmoud Mostafavi¹, Parsa Esmati¹, Maria Yankova³, Thomas F. Flint², Mike C. Smith³, Anastasia N. Vasileiou⁵, Nicolas O. Larrosa^{1,4}, Christopher E. Truman¹

¹School of Electrical, Electronic and Mechanical Engineering, University of Bristol, Queen's Building, Bristol, BS8 1TR, United Kingdom

²Henry Royce Institute, Department of Materials, Royce Hub Building, Oxford Road, Manchester, M13 9PL, United Kingdom

³Mechanical and Aeronautical Engineering Division, University of Manchester, Manchester, M13 9PL United Kingdom

⁴Tecnalia, Parque Científico y Tecnológico de Gipuzkoa, Mikeletegi Pasealekua, 2, Donostia-San Sebastián, E-20009, Spain

⁵School of Engineering, Faculty of Science and Engineering, The University of Manchester, M13 9PL, United Kingdom

ABSTRACT

Residual stresses are a crucial factor in assessing the integrity of welded joints. These stresses are known to influence the joint's strength under additional loading, with the altered grain structure at and near the joint a complicating factor. Consequently, a mesoscale model is essential to understand the accumulation of damage in components subjected to external loading, as well as the impact of prior loads on failure. This study addresses the interplay between loading direction and grain morphology, explicitly investigating damage accumulation. The mesoscale model includes a coupled crystal plasticity and a phase field fracture model to estimate the deformation induced during a laser beam weld of 316H stainless steel. The displacement boundary condition was derived from a mechanical model of the weld, with the application of the Chaboche model. The temperature field required for the grain growth and mechanical models were obtained through a thermal fluid dynamics framework. Investigation of crack initiation and propagation was carried using a phase-field fracture model, which allowed the consideration of prior loading. This study indicated that the direction of loading plays an important role in damage susceptibility. The modified grain structure based on the welding simulation showed a different strain at failure compared to the 316H stainless steel parent material. The achieved strain at failure was found to be lower in normal loading compared to the transverse direction. Presently, the crystal plasticity model fails to estimate the macroscopic residual stresses, illustrated by damage propagation resulting in earlier than expected ductile failure upon reloading. The potential causes are addressed and discussed in detail.

Keywords: ASME Conference Paper, Crystal Plasticity,

Phase Field Damage, Residual Stress, Damage, Weldments, Austenitic Stainless Steel

NOMENCLATURE

Acronyms

CPFE	Crystal Plasticity Finite Element
PFF	Phase Field Fracture
PFGG	Phase Field Grain Growth
CFD	Computational Fluid Dynamics
UMAT	User Material Subroutine
TFD	Thermal Fluid Dynamics

1. INTRODUCTION

Improving the economics of current nuclear fission reactor power stations hinges significantly on prolonging their operational lifespan. The next generation of nuclear power plants will include a focus on incorporating advanced predictive modelling alongside precise in-service testing, monitoring, and maintenance protocols. Reactor components feature a significant number of welded joints which are subjected to a range of complex loading regimes for long periods of time with large stresses at high temperatures [1]. As a result, understanding how the complexities of differing degradation techniques interact is key to understanding how component performance changes over its operational lifetime [2, 3].

Welded joints are a key design consideration due to the variability in mechanical behaviour introduced by a range of effects stemming from the welding process [4, 5]. When the weld metal is subjected to high temperatures during welding, it expands. As the welding process progresses, this molten metal cools rapidly upon exposure to the surrounding material or environment. Uneven cooling rates across the welded joint can cause non-uniform contractions, leading to the development of residual stress fields.

[†]Joint first authors

*Corresponding author: ,

These fields can elevate the susceptibility to unexpected and undesired deformation and failure by fracture mechanisms. A key focus for work within this field is to manipulate the generated residual stress fields through the use of weld processing, chemical composition, and heat treatments to give favourable properties [6–9], although finite element modelling work has shown that heat treatments are unable to fully remove residual stresses formed [10]. Within austenitic stainless steel, high temperatures can induce sensitisation in which alloying elements such as chromium and carbon can diffuse to grain boundaries where they precipitate into Cr₂₃C₆ carbides [11, 12]. This can result in the surrounding region being more susceptible to corrosion due to the local reduction in chromium content. Additionally, these carbides are much more brittle than the austenitic steel microstructure, and the difference in stiffness can result in these carbides instigating crack formation at lower levels of accumulated strain than typically seen for bulk parent material. Residual stresses can be beneficial to component performance, however, residual stresses can compromise material performance and accelerate degradation mechanisms under a range of conditions [13, 14]. Irradiation-induced defects have been observed to accumulate at greater rates in regions of large residual stresses [15], which can embrittle critical joint regions of structural components.

The measurement and determination of residual stresses is an important field to assess the behaviour of welded components and test novel heat treatments and compositions to optimise performance [16, 17]. Experimentally, this can be done through non-destructive means such as neutron scattering experiments that can measure internal residual stresses [18–26]. Near-surface measurements of type III residual stresses can be carried out using Electron Back Scatter Diffraction [27–29]. However, depending on the material and penetration depth required, X-ray diffraction techniques may be used instead [19, 25, 30–32]. Destructive methods may also be used to determine residual stresses, such as incremental hole drilling [30, 33], or the ring core method [30], both methods measure the change in dimensions of the specimen material to infer the residual stresses that have relaxed. In incremental drilling, the dimensions of a drilled hole are measured; in the ring core method, the dimensions for a cylindrical core cut from the specimen are measured. Digital image correlation can also be integrated with the above-mentioned techniques [34, 35].

Finite element modelling techniques are a common method to estimate residual stresses within a component. Finite element techniques have been widely used to model the behaviour of macro-scale component behaviour and determine macroscopic residual stresses resulting from manufacturing processes. This has been used to separate the contribution to residual stress fields from hot forming compared to that of chemical composition [36] and to determine residual stresses formed through the autofretage process for high-pressure pipes [37]. Finite element models have additionally been employed to model the relaxation of residual stresses due to mechanical loading, which has been linked to creep cavitation in steel and titanium alloys [38–40]. Additionally, within the context of welds, macroscopic weld models may be employed to examine whether isotropic or kinematic hardening laws can more accurately predict residual stress fields in weldments [41–44].

Crystal plasticity finite element (CPFE) modelling is a computational approach used to simulate the mechanical behaviour of crystalline materials at the microscopic level, combining the finite element method with crystal plasticity theory [45, 46]. It allows for the study of deformation and mechanical behaviour of polycrystalline materials. By applying CPFE to modelling residual deformation, it can capture the effects of grain-level residual stress, i.e. type II and type III. As discussed, residual stresses can exacerbate stress concentration at grain boundaries, and the relaxation of residual stresses has been linked to intergranular creep cavitation. In this area, Lindroos et al. use a phase field model to distinguish between liquid and solid phases and microsegregation on dislocation distributions and residual stresses [47]. Crystal plasticity represents a promising option for modelling this type of residual stress relaxation induced damage mechanisms on the microstructural length scale. Additionally, the capturing of grain orientation dependent behaviour makes CPFE particularly suitable to modelling residual stresses in highly textured regions such as welded regions or components made through additive manufacturing. The work of Grilli et al. used element elimination and reactivation to describe the transition between liquid and solid phases to describe the interplay between plasticity, crystallographic grain orientation, and residual stresses in the additive manufacturing process [48]. The solid/liquid field in the work of Grilli et al. was derived through computational fluid dynamics (CFD) simulations. This approach of capturing the temperature and liquid/solid fields becomes relevant, especially in mesoscale and micro-scale modelling [49, 50]. Crystal plasticity represents a flexible approach that can be applied to different loading conditions such as creep [51, 52], cyclic loading [53], or determining intergranular stress buildup during plastic deformation [54]. Crystal plasticity has also been used to determine micromechanical parameters to describe behaviour that can then be implemented into a larger scale continuum finite element model [55]. Here we present something of an inverse approach, wherein a component-scale finite element weld model provides boundary condition data to inform a crystal plasticity submodel to calculate the effect of macromechanical deformation onto the grain microstructure [56]. The grain microstructure was retrieved from a phase field model capable of grain nucleation and with consideration of anisotropy [57]. The temperature and liquid/solid field required for the grain growth model were obtained from a CFD simulation. Phase field fracture (PFF) models have been used to describe both nucleation and propagation of damage [58–60], and these approaches have also been coupled with crystal plasticity to describe damage on the microstructural length scale [61–69].

The key scientific questions to address are: what effect does the loading direction have on damage accumulation within welded microstructures? How does the interplay between loading direction and texture affect how failure occurs? Finally, what effect does the deformation resulting from the welding process, and the consequent residual stress, have on damage accumulation?

2. COMPUTATIONAL METHOD

This section contains an outline for the crystal plasticity phase field fracture (CPPFF) model implemented. The three

components of the displacement vector \mathbf{u} and the scalar damage phase field variable c are solved for using the computational process, before the Cauchy stress tensor $\boldsymbol{\sigma}$ is calculated from the deformation gradient \mathbf{F} by a process outlined in section 2.2. The MOOSE multiphysics finite element framework [70] is used, with a C++ based UMAT material subroutine. The quasi-static equilibrium problem solved within MOOSE, which neglects body forces reads:

$$\nabla \cdot \boldsymbol{\sigma} = 0. \quad (1)$$

The equations of the crystal plasticity finite element (CPFE) model have been implemented into a UMAT subroutine, which can be utilised with different solvers, including Abaqus. A more complete description of the computational method is outlined by Salvini et al. [61].

2.1 Crystal Plasticity Formulation

An integration scheme initially proposed in the work of Kalidindi [71], forms the basis of the CPFE model. A power law term was used to calculate the plastic strain rate resulting from plastic slip, similar to that of Rice et al. [72]:

$$\dot{\gamma}^\alpha = \dot{\gamma}_0^s \left(\frac{|\tau^\alpha|}{\tau_c^\alpha} \right)^{1/m_s} \text{sign}(\tau^\alpha), \quad (2)$$

where slip system independent terms $\dot{\gamma}_0^s$ and m_s denote the constant strain rate prefactor and the constant strain rate exponent respectively. In previous work, two terms, representing slip and creep, with two different power exponents and prefactors were utilized [73, 74]. However, in the present paper, dislocation slip is assumed as the main plastic deformation mechanism during the welding process and subsequent mechanical deformation. For a given slip system, α , the resolved shear stress (RSS) is denoted by τ^α , while the critical resolved shear stress (CRSS), τ_c^α , is found using [75–77]:

$$\tau_c^\alpha = \tau_c^0 + f(T)\alpha_0\mu b \sqrt{\sum_{\beta=1}^{N_s} \chi_\beta^\alpha \left(\rho_{\text{SSD}}^\beta + \left| \rho_{\text{eGND}}^\beta \right| + \left| \rho_{\text{sGND}}^\beta \right| \right)}, \quad (3)$$

where:

$$f(T) = k_A + k_B e^{-k_C(T-T_0)} \quad (4)$$

where τ_c^0 is a constant Peierls stress, the stress required to move a dislocation within a plane of atoms, α_0 is the Taylor hardening prefactor, μ is the shear modulus, b the Burgers vector length, and $f(T)$ a prefactor that accounts for temperature dependent changes in hardening behaviour [48], where k_A , k_B , k_C are constants, and T_0 is room temperature. Three state variables are used to describe the total dislocation density within each slip system, these are: ρ_{SSD}^α , the statistically stored dislocation (SSD) density, $\rho_{\text{eGND}}^\alpha$ and $\rho_{\text{sGND}}^\alpha$, which represent the density of geometrically necessary dislocations (GND) with subscripts to denote respective edge and screw character. The interaction hardening effect caused by one slip system, β , on another, α , is denoted by χ_β^α [78, 79]. For an FCC crystal structure, this is described by a symmetric 12×12 matrix whose entries represent interactions between slip systems. The values of χ_β^α implemented are defined in eqn. 5, assuming a

unity hardening factor in coplanar slip system interactions, and a constant value of 1.4 otherwise.

$$\chi_\beta^\alpha = \begin{cases} 1 & \text{if } \alpha = \beta, \\ 1.4 & \text{if } \alpha \neq \beta, \end{cases} \quad (5)$$

Time evolution of SSD density ρ_{SSD}^α encompasses both dislocation multiplication annihilation [80, 81]:

$$\dot{\rho}_{\text{SSD}}^\alpha = \left(k_m \sqrt{\rho_{\text{SSD}}^\alpha + \left| \rho_{\text{eGND}}^\alpha \right| + \left| \rho_{\text{sGND}}^\alpha \right|} - 2y_c \rho_{\text{SSD}}^\alpha \right) \frac{|\dot{\gamma}^\alpha|}{b}, \quad (6)$$

the dislocation accumulation rate and the experimentally determined critical annihilation distance for adjacent dislocations are denoted k_m and y_c respectively [82]. By comparing stress-strain curves between simulation results and experimental data, parameters in equation 6 reproduce hardening and saturation in FCC metals. GND density evolution is calculated with slip gradient projections along the slip direction and the edge dislocation line direction, s^α and t^α respectively [83–85]:

$$\dot{\rho}_{\text{eGND}}^\alpha = -\frac{1}{b} \nabla \dot{\gamma}^\alpha \cdot s^\alpha, \quad (7)$$

$$\dot{\rho}_{\text{sGND}}^\alpha = \frac{1}{b} \nabla \dot{\gamma}^\alpha \cdot t^\alpha. \quad (8)$$

2.2 Phase Field Damage Formulation

Phase field damage is used in this work for its ability to model arbitrary crack propagation, which is advantageous in the case of stainless steel welds, in which the crack can be both intergranular and intragranular, depending on the thermal history and amount of carbides. Other common techniques such as cohesive zone model are more suitable when the crack is intergranular only [86–89].

Damage nucleation and propagation during plastic deformation is calculated using the implemented phase field damage model, which is coupled with the crystal plasticity formulation described in section 2.1. Based on a continuum damage variable, $c = 0$ represents undamaged material and $c = 1$ represents totally damaged material [61, 68, 90, 91]. The phase field fracture model is similar to that of Grilli et al. [92–94], based on the elastic strain energy, albeit with a modification to include the plastic work into the damage evolution law. This model implements a free energy formulation, where the free energy per unit volume, Ψ , is the sum of the mechanical part Ψ_m and the energy released, Ψ_f , forming fracture surfaces,

$$\Psi = \Psi_f + \Psi_m. \quad (9)$$

The free energy per unit volume is dependent upon the elastic deformation gradient \mathbf{F}_e . A dissipation function \mathcal{D} is utilised, incorporating the plastic work rate \dot{W}_p as proposed by Lee [95, 96]:

$$\mathcal{D}(\mathbf{F}_e, \mathbf{F}_p, \dot{\mathbf{F}}_p) = \dot{W}_p = \int_V \text{tr}(\boldsymbol{\sigma} \mathbf{F}_e \dot{\mathbf{F}}_p \mathbf{F}_p^{-1} \mathbf{F}_e^{-1}) \det(\mathbf{F}_e) dV. \quad (10)$$

For the monotonic loads used within this work, W_p is a monotonically increasing function representing the total plastic work

done. Overall, the second Piola-Kirchhoff stress tensor S is derived by equations 11 and 12 in two cases determined by the value of the determinant of the elastic deformation gradient, J_e . Under compression, when $J_e < 1$, the following is used:

$$S = [(1 - c)^2 + k_r] \mathbb{C} : E_e \quad (11)$$

Meanwhile, during expansion, when $J_e \geq 1$, the following is instead used:

$$S = [(1 - c)^2 + k_r] (\mathbb{C} : E_e - J_e^{2/3} K \omega C_e^{-1}) + J_e^{2/3} K \omega C_e^{-1} \quad (12)$$

where the elastic volumetric expansion is denoted by ω [61], and \mathbb{C} is varied to allow for temperature dependent changes of the stiffness matrix during the weld process and as the structure cools similar to that of Grilli et al. [48]:

$$C_{ij}(T) = C_{ij}(T_0) \left(1 - \frac{dC_{ij}}{dT}(T - T_0) \right). \quad (13)$$

It should be noted that \mathcal{D} is not dependent on the time derivative of E_e , therefore not contributing to the stress tensor [95]. On the other hand, since \mathcal{D} depends on the phase field damage, c , the plastic work will affect the time evolution of c . The stress degradation under tensile loading denotes a reduction in stiffness, interpretable as voids within the system. The minimisation of the free energy density, Ψ , and the dissipation function \mathcal{D} determines the evolution of c , using a rate-dependent approach based on an Allen-Cahn equation:

$$\dot{c} = \frac{1}{\eta} \left\langle l_0 \Delta c - \frac{c}{l_0} + 2(1 - c) \frac{(a^+ + \beta W_p)}{G_c} \right\rangle \quad (14)$$

where η is a kinetic coefficient and $\langle \rangle$ are McCauley brackets, such that $\langle x \rangle = x$ if $x > 0$ and $\langle x \rangle = 0$ if $x < 0$. The critical energy release rate for fracture as defined by Griffith's theory is represented by G_c [97], and the characteristic regularisation length-scale which dictates the diffusiveness of the damage field is represented by l_0 . β is a constant.

2.3 Thermal Fluid Dynamics and Grain Growth Model

A mesoscale computation of residual stresses necessitates microstructural information concerning grain size, morphology and orientation, the estimation of which requires the thermal history of the component. Comparable modelling strategies have been established and verified in the contexts of welding and additive manufacturing processes [48, 98]. The computation of the temperature field relies on understanding the characteristics of the molten pool. This arises from the temperature field's dependence on the state of material. A thermal fluid dynamics (TFD) model, solving the coupled momentum and energy equations, is used for this purpose [99, 100]. Specifically, a laser beam welding process is simulated in which the laser power is 7296 W and the scanning speed is 4.16 mm.s⁻¹. An OpenFOAM based code, called LaserbeamFoam, is used for this purpose [100]. This coupled approach results in the temperature field of the domain and the corresponding fluid fraction. The microstructure is captured by solving a phase field grain growth (PFGG) model, which uses as input the temperature field produced by TFD simulations.

A non-conservative order parameter is chosen to represent the grains based on the grain orientation. The evolution of these parameters is formulated by a time-dependent Ginzburg-Landau equation [101]. Phase field techniques are ideal for this purpose because they can capture the anisotropic behavior of interfaces [102–104], which is included also in the present model. The orientations are then transformed into the angle ϕ_1 illustrated in figure 1. Two different initial grain sizes, 30 μm and 60 μm, representing different microstructures in the parent material, are used to generate two different final microstructures, which will be used in the subsequent CPPFF weld process simulations.

3. MATERIALS

3.1 Material Parameters and Mechanical Properties

The material simulated was 316H stainless steel. The input parameters for the crystal plasticity model were found using an iterative Nelder-Mead algorithmic process comparing the simulated output stress strain response to experimental stress strain curves obtained from the literature. The critical energy release rate G_c used within the phase field fracture model during the mechanical load was based on a value determined for 550°C in [61], which compared the strain for failure under monotonic tensile loading to the experimentally observed value for 316H steel, while the value of G_c is set as much larger during the welding process stage, to avoid the formation of hot cracking, which is not commonly observed in stainless steel laser welds [105]. The high-temperature gradients and the thermal cycles induced during welding result in deformations and stresses within the component. A modelling technique is essential for estimating the resultant stresses and deformations at the component scale. The Chaboche model is particularly suitable, given its capability to capture cyclic plasticity and kinematic hardening [106]. Hence, the Chaboche model, implemented within a finite element analysis framework, was adopted to estimate the deformations associated with the thermal expansions and contractions. The corresponding calibration is reported in [42]. The extracted strain components are applied to the CPPFF simulations of the welding process using a submodeling approach.

3.2 Microstructure

The output from the phase field grain growth model provided the grain orientation, expressed with three Euler angles, in a structured mesh on an element-by-element basis. The PFGG was carried out for two initial grain sizes (d_0) of 30 μm and 60 μm, the results of which are compared. The quaternion rotations for each element were used to determine the three Euler angle rotations in the "ZXZ" convention, which could be used to reconstruct the generated microstructure within the crystal plasticity finite element framework. The microstructures were sampled at frequency of every five elements to reduce the size of the microstructure to reduce the computational cost of the CPPFF simulations, resulting in the final simulated microstructures shown in figure 1.

4. SIMULATION PROCEDURE

Estimation of the displacement was done with the Chaboche model outlined in 3.1. The temperature profile generated by the thermal model was used within the Chaboche model to obtain

TABLE 1: Input parameters used within the crystal plasticity phase field fracture model for 316H stainless steel

Model Parameter	Value
Number of Elements	2400
Elastic constant (\mathbb{C}_{11}) at $T = T_0$	204.6 GPa
Elastic constant (\mathbb{C}_{12}) at $T = T_0$	137.7 GPa
Elastic constant (\mathbb{C}_{44}) at $T = T_0$	126.2 GPa
Derivative of Elastic Constant ($d\mathbb{C}_{11}/dT$)	0.0004415 GPa K ⁻¹
Derivative of Elastic Constant ($d\mathbb{C}_{12}/dT$)	0.0003275 GPa K ⁻¹
Derivative of Elastic Constant ($d\mathbb{C}_{44}/dT$)	0.000410 GPa K ⁻¹
Shear modulus (μ)	91.9 GPa
Initial SSD density (ρ_{SSD}^α)	17.08 μm^{-2}
Initial GND Density - Edge ($\rho_{eGND}^\alpha (t = 0)$)	0.0 μm^{-2}
Initial GND Density - Screw ($\rho_{sGND}^\alpha (t = 0)$)	0.0 μm^{-2}
Reference Slip Rate ($\dot{\gamma}_0^s$)	0.001 s ⁻¹
Slip strain rate sensitivity exponent (m_s)	0.1
Peierls stress (τ_c^0) at $T = T_0$	0.112 MPa
Temperature dependence of CRSS (k_A)	0.53
Temperature dependence of CRSS (k_B)	0.47
Temperature dependence of CRSS (k_C)	0.008
Burgers vector length (b)	0.256 nm
Taylor hardening prefactor (α_0)	0.3
Dislocation accumulation rate (k_m)	1.13
Dislocation Capture Radius (y_c)	1.3 nm
Room temperature (T_0)	293 K
Characteristic Phase Field Model Length-scale (l_0)	67.0 μm
Critical Energy Release Rate (G_c)	6200 Jm ⁻²
Damage kinetic coefficient (η)	0.001 sm ⁻¹
Damage plastic work contribution prefactor (β)	0

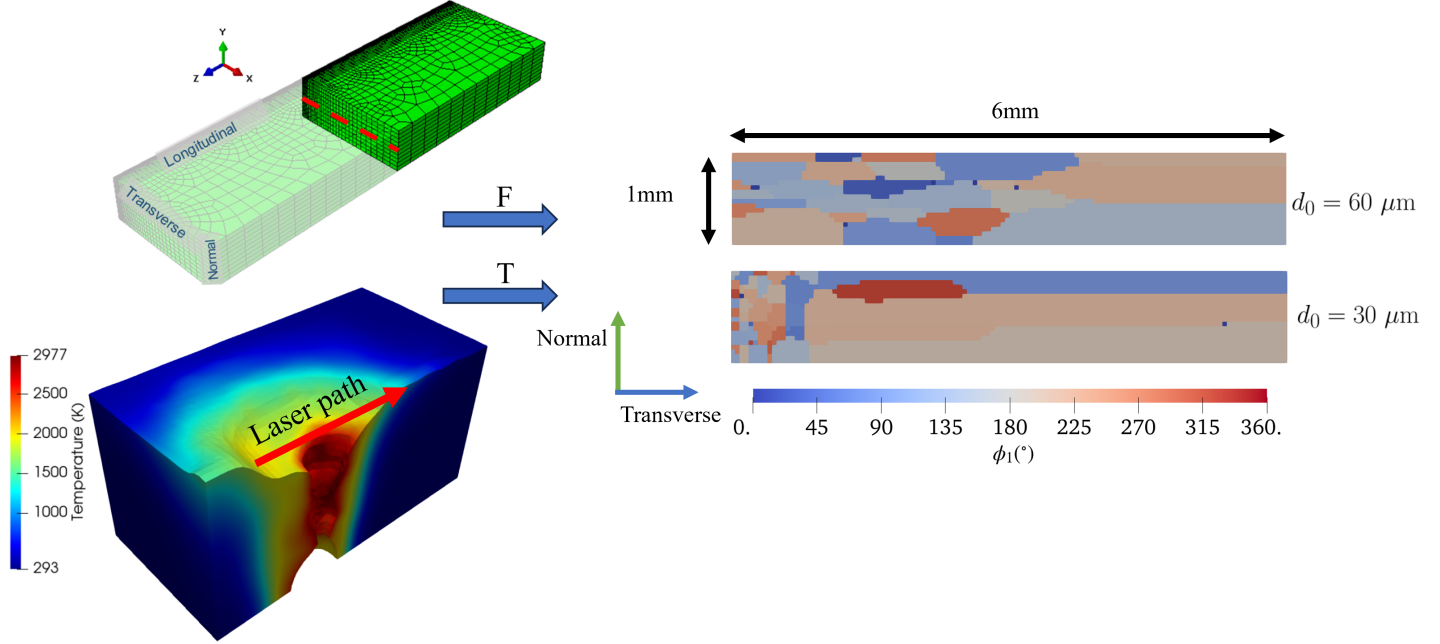


FIGURE 1: The deformation gradient (F) and the temperature field (T) from the finite element model and TFD model are used to estimate the temperature and, in turn, the microstructure using PF GG, with two initial grain sizes.

the strain field due to thermal expansion. The resultant strain was multiplied by the corresponding length of the domain to retrieve the displacement field. The consequent displacement was implemented as the boundary condition required for the crystal plasticity submodel. The boundary condition displacements for the entire loading history are shown in figure 3a, a schematic of the implemented boundary conditions and defined loading directions relative to the weld direction is shown in figure 2.

To ensure boundary conditions were smoothly applied and avoid convergence issues relating to exceeding slip increment tolerances within the crystal plasticity model, a smoothing fit was applied to the period during which a significant portion of the loading occurs. Figure 3b shows the boundary conditions during the time of interest. The boundary conditions during the first stage of the welding process were applied as displacements imposed as a function of time to the positive faces in the weld transverse and weld normal directions, seen in figure 2 as the schematic labelled a). The negative faces in these directions were fixed at zero normal displacement, i.e. roller boundary conditions, while the other faces were left free. Following the weld deformation loading, after the system has cooled down to room temperature, shown in figure 3b, the boundary conditions were altered to leave the loading faces free, allowing for relaxation of the specimen, see b) in figure 2. After sufficient time was allowed for the specimen to mechanically relax, the specimen was reloaded in directions either transverse or normal to the weld direction. Due to heterogeneous relaxation of the specimen along the loading faces, i.e. surfaces not being flat at the grain length scale, the previous displacement time boundary conditions could not be used. Instead, a velocity set boundary condition was applied in which each element on a chosen face was assigned a velocity, equivalent to increasing strain by 0.001s^{-1} in either in the weld

normal or transverse directions. A representation of this loading is shown in c) of figure 2. Two different types of simulations are carried out, in which the load is along the transverse or along the normal direction only.

5. RESULTS

Within sections 5.1, 5.2, and 5.3, results are distinguished by the different directions that reloading occurs in. The directions are named as either normal or transverse to the weld direction as described in section 3.2 and shown in figure 1.

5.1 Change in Ductility

The microstructures were subjected to tensile loading until the damage phase field had developed to show crack propagation which was taken to be the point at which the material had failed. The total strain was calculated by comparing the deformed microstructure to the original microstructure and by summing all the strain increments imposed on the system, both during the welding process and during reload. This was used to determine the strain for failure once crack propagation had been achieved, accounting for both the initial deformation as well as deformation due to reloading. Respective strain for failure values were found for the two microstructures with different grain sizes when loaded in the normal and transverse directions. This was compared to a parent material microstructure, which had an average two dimensional grain diameter of $44\mu\text{m}$. The strain for failure values can be seen in figure 4. The model predicts that a larger initial grain size will result in a higher strain for failure, which agrees with experiments, as reported later in the discussion section. This is true both when the system is loaded in a direction transverse or normal to the weld. The model also predicts that the strain for failure is reduced for weld microstructures with residual stresses compared to an untextured parent microstructure.

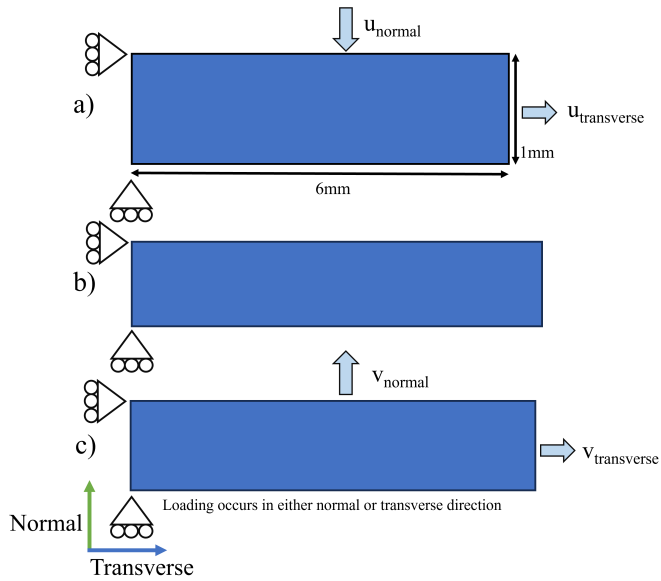


FIGURE 2: A schematic detailing the three simulation stages, with: a) indicating the initial deformation obtained from the Chaboche model; b) indicating stress relaxation as displacement boundary conditions are removed; and c) indicating the reloading either in the normal or transverse directions.

5.2 Damage Accumulation

The damage phase fields for the $d_0 = 30\mu\text{m}$ weld microstructure was compared at different levels of strain upon reloading in the weld transverse and normal directions. The damage phase field can be seen in figure 5, which show that for normal loading, damage accumulation is more focused along elongated grain boundaries perpendicular to the loading direction. If the loading is transverse to the weld, damage grows and propagates within the smaller grains of the heat affected zone (HAZ). The crack path can be seen overlaid on the weld microstructure for the two loading directions in figure 6, showing that the phase field growth at lower strain matches the regions where eventual fracture occurs.

5.3 Mechanical Stress Response

To understand the residual stress field after the relaxation stage, the stress tensor was extracted along a line in the middle of the region along the transverse direction, and the stress components in transverse and normal directions were plotted against the distance from the fusion zone for the two microstructures in Figures 7 and 8. The magnitude of the residual stress is of the order of hundreds of MPa and there are several positive and negative peaks, showing the transition from one grain to the other. These values are comparable to those observed within the literature for 316H weldments [41, 107]. The normal direction residual stress in Figure 8 shows more positive peaks compared to the transverse direction residual stress in Figure 7 for both grain sizes. This positively correlates with the lower ductility exhibited during load along the normal direction, as shown in Figure 4.

Upon subsequent reloading, the average stress in the loading direction was plotted against loading time, as shown in figure 9. The yield stress is unchanged by the difference in loading

direction, except for the $d_0 = 30\mu\text{m}$. This was expected due to the level of accumulated hardening in this simulation compared to the others. Since the elastic properties are varied as a function of the phase field damage (see (15)), a greater level of damage can be expected to result in later yielding, as well as differences in the observed elastic behaviour:

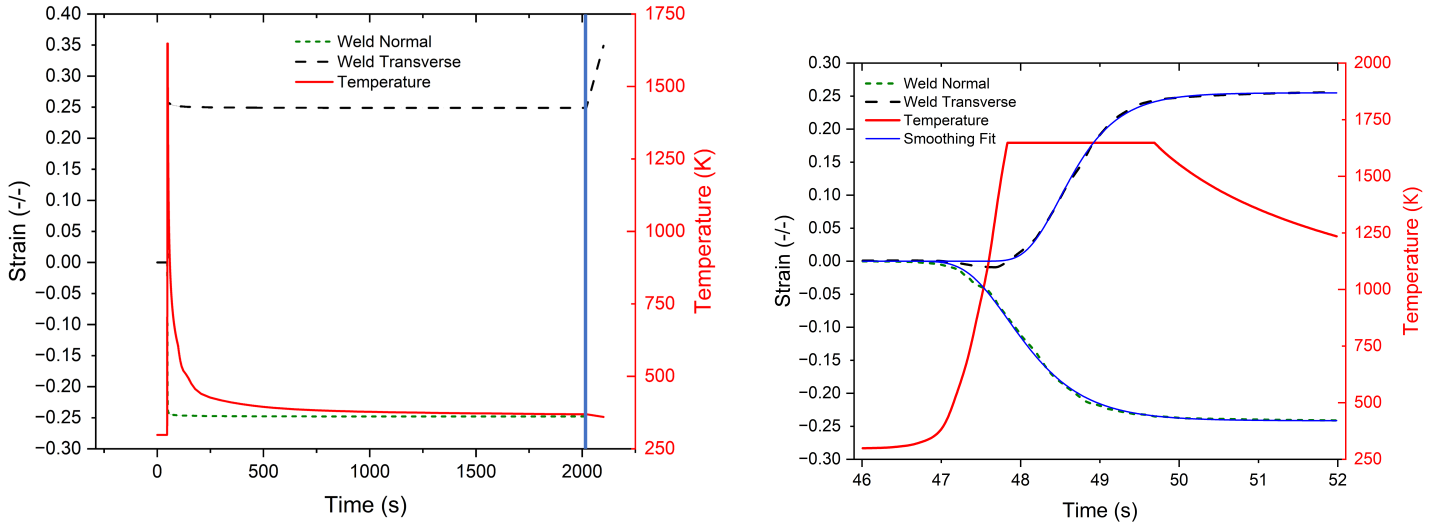
$$\mathbb{C}(T) \rightarrow (1 - c^2)\mathbb{C}(T) \quad (15)$$

6. DISCUSSION

The modelling presented here shows that depending on loading direction, the total elongation including the deformation resulting from the welding process is between 19% and 25%. When only the strain induced by reloading after relaxation is considered, failure occurs at between 5% and 10%, showing that the model is underestimating the ductility of 316H weldments. There are a number of possible reasons for this disparity relating to the modelling approach used, which can be associated with either the crystal plasticity model or the phase field fracture model.

It has been discussed within the literature that under a range of loading conditions, the failure behaviour of austenitic steel weldments, and those of 316H in particular is determined by phase composition and the presence of intergranular carbides of type $M_{23}C_6$. This effect has been described for both ductile creep failure and ductile failure [108, 109]. Additionally, the presence of δ ferrite phases affects the ductile behaviour of weldments, and weldments can subsequently exhibit greater ductility from the ability to relieve residual stresses through gross plasticity. Subsequent ageing of weldments also has a significant effect on the ductility behaviour, particularly in the case of 316H due to the changes in phase behaviour [110]. Such microstructural behaviour has not been accounted for within this model. Furthermore, the elastic modulus and yield stress for weldments varies significantly from unwelded parent material because of microstructural evolution and macroscopic residual stresses that must be overcome. Within the plasticity model presented, variation in elastic properties and hardening behaviour due to sample temperature has been accounted for as shown in (4) and (13). However, a more representative approach to the problem presented would allow for adjustment of elastic properties based on residual stress during the relaxation phase. Additionally the strain at failure was observed to increase with the grain size as illustrated in Figure 4. The models with a grain size of $60\mu\text{m}$ tend to have a higher aspect ratio, which can be observed in Figure 1. The increase in strain at failure is in agreement with the work of Wilson-Heid et al. [111]. Their research indicates enhanced ductility in columnar grains, which are a result of continuous-wave laser additive manufacturing, in contrast to the equiaxed grains that form in Ti-6Al-4V when subjected to pulsed laser treatment. Similar observations are made in the work of Guercio et al. on the study of cracking behaviour in AA2025 in laser powder bed fusion [112]. The model presented simulated a two-dimensional slice of material from a larger simulation. In this case, the crystal plasticity model is unable to capture the wider effect of the bulk on the simulated region.

Other issues arise from the phase field fracture model employed from this work. The fracture driving force formulation



(a) The entire load history applied. The blue line indicates the time at which reloading begins, the example here is for reloading in the direction transverse to the weld.

(b) A more detailed view of the applied deformation in the time range of significant thermal strain induced deformation.

FIGURE 3: The deformation applied over time to the submodel during the weld process. Normal and transverse refer to the directions that are normal and transverse to the weld direction in the weld model.

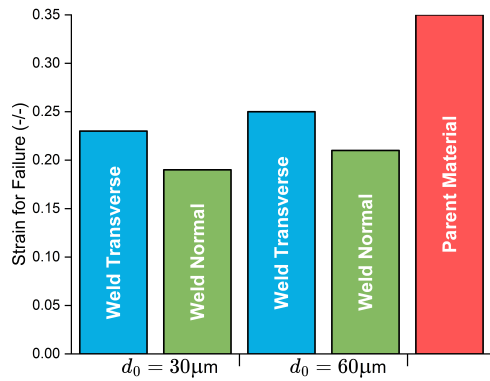


FIGURE 4: The total strain for failure for weld microstructures relative to before any deformation, i.e. strain is the sum of thermal deformation induced strain and applied strain, with varying initial grain size for loading in transverse and normal directions to the weld, compared to an untextured parent microstructure.

is based upon the elastic strain energy density, which in turn is based upon the deformation gradient. As the weld deformation progresses, the fracture driving force is directly tied to the amount of accumulated deformation. In reality, the weldment is either in a liquid phase at high temperature or solidifying, and thus accumulating damage in this period would not make physical sense. The approach taken in this work to alleviate this issue is to implement a variable factor G_c in (14), which describes the energy density to form a crack. While this can reduce the amount of damage formed during the weld deformation phase, as the sample is allowed to relax and the value of G_c is decreased

to allow for meaningful loading damage accumulation behaviour, the underlying fracture driving force remains, causing the phase field damage to rapidly increase. For subsequent loading, the form of (14) includes other driving force terms such as a phase field gradient dependent term. Typically, when modelling crack propagation, this term localises crack evolution to regions of existing crack formation. If the phase field is at a high level and diffuse, the damage continues to grow faster than otherwise expected (see section 5.2), leading to the aforementioned issues with premature fracture as the weldment undergoes reloading. Several methods were explored to best mitigate this issue, which included simulating the initial weld deformation and relaxation using a separate crystal plasticity model, before using importing state variables for deformation, stress, and hardening into a new simulation with different boundary conditions with the phase field fracture model acting. This implementation encountered issues with convergence. Instead, the approach using the coupled crystal plasticity phase field fracture model was used with dynamic boundary conditions with an inertia term that prevented sudden changes in boundary conditions, improving convergence.

The model predicts that for both normal and transverse loading directions, the microstructure with the smaller initial grain size results in a lower strain for failure compared to a larger grain size structure, matching experimental observations for 316H [113]. The model also shows a difference in strain for failure between loading in the transverse and normal weld directions, but experimental validation from the literature is required. This could be explained by the orientation of grain boundaries within the heat affected zone relative to the loading direction. If loading is in the normal direction in a region of columnar grains, the average distance between grain boundaries for dislocation slip is lower compared to loading in a perpendicular direction. The compressive residual stresses observed within the grains at the

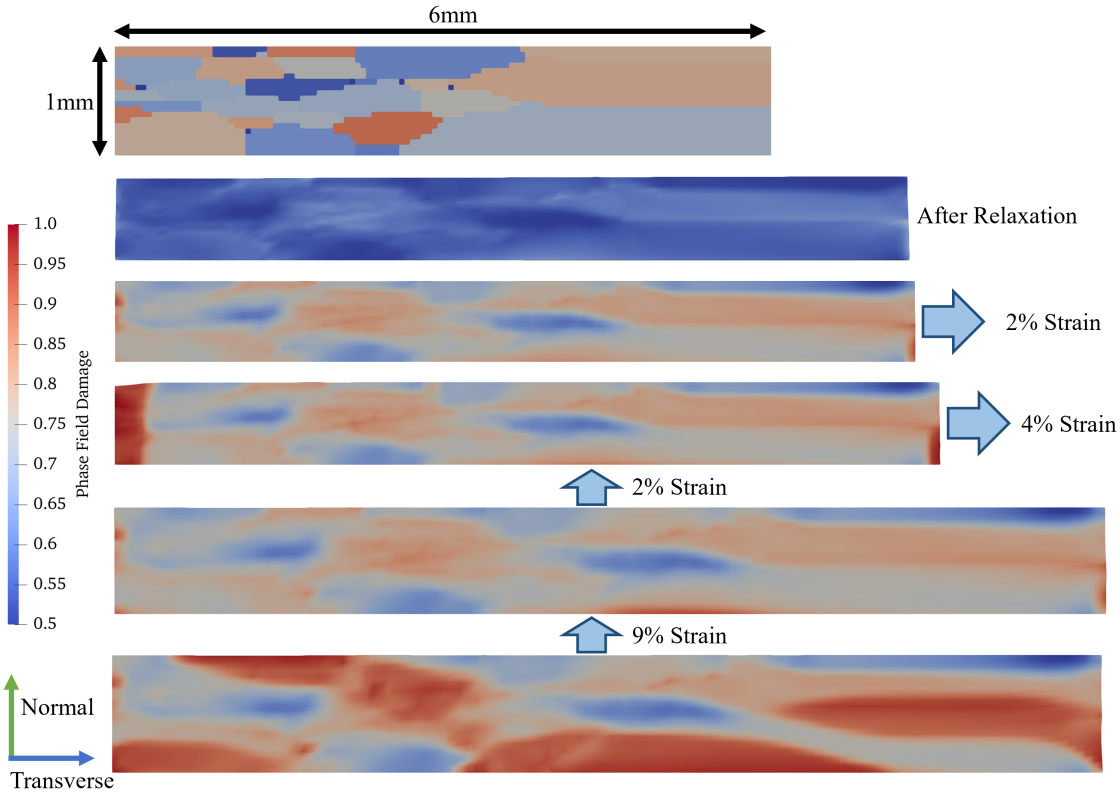


FIGURE 5: The phase fields displaying the level of damage accumulation depending on the level of strain when loaded either normal or transverse to the weld direction for a generated microstructure with initial grain size $d_0 = 60\mu\text{m}$.

edge of the heat affected zone where crack initiation occurs, seen in Figure 7, must be relieved by tensile stress during reloading and can explain the change in strain at failure simulated. The $d_0 = 30\mu\text{m}$ microstructure with smaller grains had a larger oscillating and tensile stress along the normal direction than the $d_0 = 60\mu\text{m}$ microstructure, suggesting that it has a stress state closer to yield and potential ductile failure. The difference in stress state can account for the discrepancy in strain at failure between the two microstructures for reloading in both the transverse and normal directions.

7. CONCLUSION

An application for modelling the effect of deformation in the centre of a laser weld is implemented from a thermal fluid flow weld model to a crystal plasticity submodel to predict the effect of grain-to-grain residual stresses upon relaxation. Further work studies the effect of this prior loading on damage accumulation within a microstructure subjected to subsequent tensile load in directions that are normal or transverse to the weld direction. This is explored through a coupled crystal plasticity phase field fracture model. The model predicts a reduction in strain for failure for weld generated microstructures compared to parent 316H stainless steel, with normal direction loading resulting in a lower strain for failure.

Simulations show that the regions susceptible to damage propagation depends on the direction of loading, which exac-

erbates effects pertaining to grain morphology and orientation relative to the loading direction. It was found that loading transverse to the weld instigates damage within the smaller grains at the edge of the heat affected zone (HAZ), whereas normal direction loading is more focused along the elongated boundaries of columnar grains perpendicular to the load direction. The subsequent crack paths once ductile failure has occurred show that these regions of initial damage coalescence are indicative of the final crack path, with transverse direction loading leading to a larger strain for failure than normal loading, although both loading directions were found to underestimate the strain for failure upon reloading compared to literature data.

The stress field upon relaxation was averaged over the simulated region to determine the residual stress remaining, finding that larger compressive residual stress within the smaller grains at the edge of the HAZ suppressed ductile failure. The residual stress in both simulated microstructures was found to be below results predicted by continuum finite element models of laser welded 316H steel [107], and the $d_0 = 30\mu\text{m}$ with smaller grains showed larger peaks of tensile residual stress than the microstructure with larger grains, suggesting that it was closer to the yield stress and can explain why the smaller grain microstructure failed at a lower elongation.

Key difficulties within the CPFE PFF modelling framework for this type of weld simulation have been identified, such as the driving force basis in the deformation gradient causing earlier

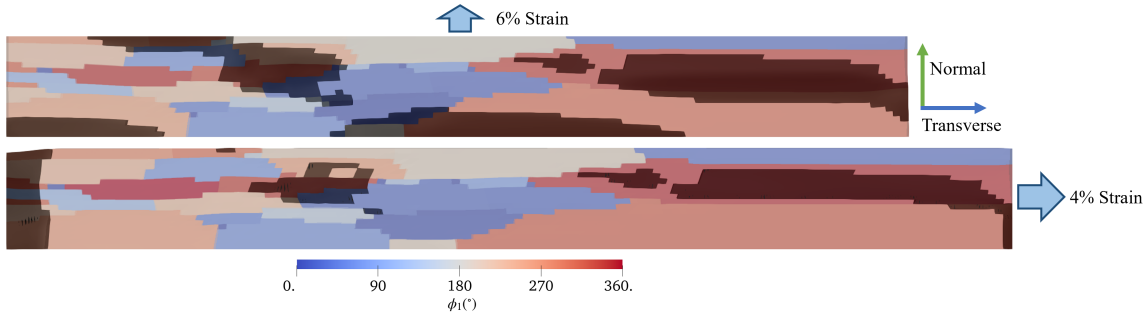


FIGURE 6: The simulated microstructure for the larger grain microstructure $d_0 = 60\mu\text{m}$ after fracture has occurred. The phase field representing the crack path is shown in black over the microstructure grain orientations represented by different colours.

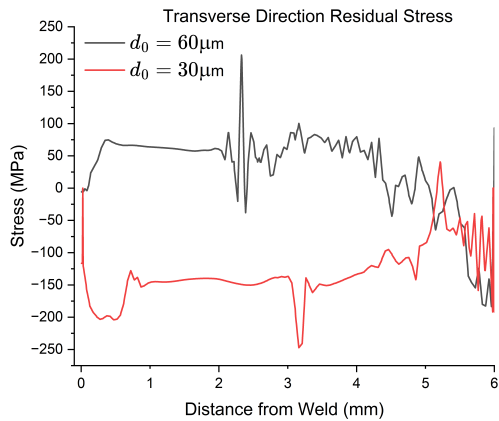


FIGURE 7: The residual stress in the transverse direction plotted as a function of the distance from the centre of the weld, comparing the two simulated microstructures.

than expected ductile failure, and that the boundary conditions implementable within crystal plasticity in this form are unable to capture macroscopic residual stresses acting across the simulated microstructure. Not capturing this behaviour is also expected to contribute to the lower-than-expected ductility of the weldments.

ACKNOWLEDGEMENTS

M.S. acknowledges the support by the EPSRC Center for Doctoral Training in Nuclear Energy Futures. P.E. acknowledges the support by EPSRC DTP scholarship. M.M., D.K., E.D., N.G. acknowledge the support by the SINDRI partnership, EPSRC grant EP/V038079/1.

REFERENCES

- [1] Pandey, Chandan, Mahapatra, Manas Mohan, Kumar, Pradeep and Saini, Nitin. “Some studies on P91 steel and their weldments.” *Journal of Alloys and Compounds* Vol. 743 (2018): pp. 332–364. DOI <https://doi.org/10.1016/j.jallcom.2018.01.120>. URL <https://www.sciencedirect.com/science/article/pii/S092583881830121X>.
- [2] Odette, G. Robert and Zinkle, Steven J. “Structural Alloys for Nuclear Energy Applications.” Elsevier, Boston

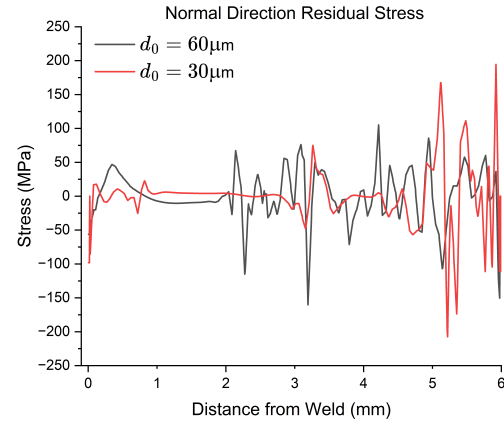


FIGURE 8: The residual stress in the normal direction plotted as a function of the distance from the centre of the weld, comparing the two simulated microstructures.

(2019): p. iv. DOI <https://doi.org/10.1016/B978-0-12-397046-6.09995-0>. URL <https://www.sciencedirect.com/science/article/pii/B9780123970466099950>.

- [3] Irastorza-Landa, Ainara, Grilli, Nicolò and Swygenhoven, Helena Van. “Effect of pre-existing immobile dislocations on the evolution of geometrically necessary dislocations during fatigue.” *Modelling and Simulation in Materials Science and Engineering* Vol. 25 No. 5 (2017): p. 055010. DOI [10.1088/1361-651X/aa6e24](https://doi.org/10.1088/1361-651X/aa6e24). URL <https://dx.doi.org/10.1088/1361-651X/aa6e24>.
- [4] Deng, Dean, Murakawa, Hidekazu and Liang, Wei. “Numerical and experimental investigations on welding residual stress in multi-pass butt-welded austenitic stainless steel pipe.” *Computational Materials Science* Vol. 42 No. 2 (2008): pp. 234–244. DOI <https://doi.org/10.1016/j.commatsci.2007.07.009>. URL <https://www.sciencedirect.com/science/article/pii/S0927025607001978>.
- [5] Pang, Yong, Grilli, Nicolò, Su, Hang, Liu, Wencheng, Ma, Jun and Yu, Siu Fung. “Experimental investigation on microstructures and mechanical properties of PG4 flash-butt rail welds.” *Engineering Fail-*

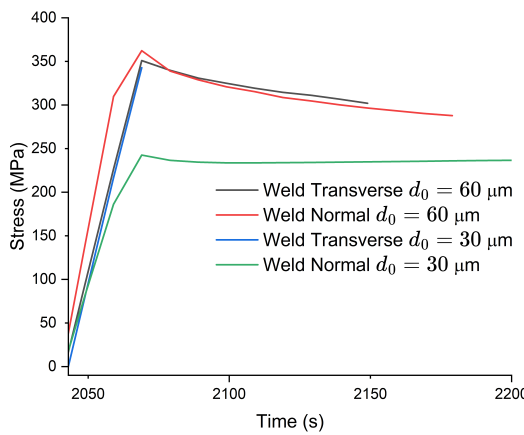


FIGURE 9: The loading direction stress upon reloading over the two generated microstructures when loaded in directions that are transverse and normal to the weld direction.

- ure Analysis Vol. 141 (2022): p. 106650. DOI <https://doi.org/10.1016/j.engfailanal.2022.106650>. URL <https://www.sciencedirect.com/science/article/pii/S1350630722006227>.
- [6] Coules, H. E. “Contemporary approaches to reducing weld induced residual stress.” *Materials Science and Technology* Vol. 29 (2013): pp. 4–18. DOI [10.1179/1743284712Y.0000000106](https://doi.org/10.1179/1743284712Y.0000000106). URL <https://www.tandfonline.com/doi/abs/10.1179/1743284712Y.0000000106>.
- [7] Akyel, F., Gämmerdinger, M., Olschok, S., Reisgen, U., Schwedt, A. and Mayer, J. “Adjustment of chemical composition with dissimilar filler wire in 1.4301 austenitic stainless steel to influence residual stress in laser beam welds.” *Journal of Advanced Joining Processes* Vol. 5 (2022): p. 100081. DOI <https://doi.org/10.1016/j.jajp.2021.100081>. URL <https://www.sciencedirect.com/science/article/pii/S2666330921000418>.
- [8] De Risi, R., Moody, T., Voyagaki, E., Gunner, S., Pregnolato, M., Grilli, N. and Taylor, C. *Multi-scale structural integrity assessment of a series of identical components in cultural-heritage structures: The case of the Clifton suspension bridge*. CRC Press (2023).
- [9] Raghunathan, V. S., Seetharaman, V., Venkadesan, S. and Rodriguez, P. “The influence of post weld heat treatments on the structure, composition and the amount of ferrite in type 316 stainless steel welds.” (1979). DOI [10.1007/BF02811701](https://doi.org/10.1007/BF02811701). URL <https://link.springer.com/article/10.1007/BF02811701>.
- [10] Yaghi, Anas H., Hyde, Thomas H., Becker, Adib A., Sun, Wei, Wen, Wu, Hilson, Gabrielle, Simandjuntak, Sarinova, Flewitt, Peter EJ., Pavier, Martyn J. and Smith, David J. “Comparison of measured and modelled residual stresses in a welded P91 steel pipe undergoing post weld heat treatment.” *International Journal of Pressure*

Vessels and Piping Vol. 181 (2020): p. 104076.

DOI <https://doi.org/10.1016/j.ijpv.2020.104076>.

URL <https://www.sciencedirect.com/science/article/pii/S0308016120300545>.

- [11] Martin, Tomas, He, Siqi, Horton, Edward, Shang, Hao, Fernandez-Caballero, Antonio, Grilli, Nicolo, Mostafavi, Mahmoud, Knowles, David, Cocks, Alan and Flewitt, Peter. “New Correlative Microscopy Approaches to Understand the Microstructural Origins of Creep Cavitation in Austenitic Steels.” *Microscopy and Microanalysis* Vol. 28 (2022): pp. 2074–2075. DOI [10.1017/S1431927622008030](https://doi.org/10.1017/S1431927622008030). URL <https://www.cambridge.org/core/journals/microscopy-and-microanalysis/article/new-correlative-microscopy-approaches-to-understand-the-microscopic-origins-of-creep-cavitation-in-austenitic-steels/C796F10FEBDC359EDD65E10262A3438A>.
- [12] Beckett, F.R. and Clark, B.R. “The shape and mechanism of formation of M₂₃C₆ carbide in austenite.” *Acta Metallurgica* Vol. 15 No. 1 (1967): pp. 113–129. DOI [https://doi.org/10.1016/0001-6160\(67\)90159-9](https://doi.org/10.1016/0001-6160(67)90159-9). URL <https://www.sciencedirect.com/science/article/pii/0001616067901599>.
- [13] Turski, M., Bouchard, P.J., Steuwer, A. and Withers, P.J. “Residual stress driven creep cracking in AISI Type 316 stainless steel.” *Acta Materialia* Vol. 56 No. 14 (2008): pp. 3598–3612. DOI <https://doi.org/10.1016/j.actamat.2008.03.045>. URL <https://www.sciencedirect.com/science/article/pii/S1359645408002498>.
- [14] Grilli, Nicolò, Cocks, Alan C.F. and Tarleton, Edmund. “Crystal plasticity finite element modelling of coarse-grained α -uranium.” *Computational Materials Science* Vol. 171 (2020): p. 109276. DOI <https://doi.org/10.1016/j.commatsci.2019.109276>. URL <https://www.sciencedirect.com/science/article/pii/S0927025619305750>.
- [15] Stoenescu, R., Schäublin, R., Gavillet, D. and Baluc, N. “Welding-induced microstructure in austenitic stainless steels before and after neutron irradiation.” *Journal of Nuclear Materials* Vol. 360 (2007): pp. 186–195. DOI [10.1016/J.JNUCMAT.2006.10.007](https://doi.org/10.1016/J.JNUCMAT.2006.10.007).
- [16] Chen, Wen, Voisin, Thomas, Zhang, Yin, Florien, Jean-Baptiste, Spadaccini, Christopher M, McDowell, David L, Zhu, Ting and Wang, Y Morris. “Microscale residual stresses in additively manufactured stainless steel.” *Nature communications* Vol. 10 No. 1 (2019): pp. 1–12.
- [17] Xiong, Yi, Karamched, Phani S., Nguyen, Chi-Toan, Collins, David M., Grilli, Nicolò, Magazzeni, Christopher M., Tarleton, Edmund and Wilkinson, Angus J. “An in-situ synchrotron diffraction study of stress relaxation in titanium: Effect of temperature and oxygen on cold dwell fatigue.” *Acta Materialia* Vol. 213 (2021): p. 116937. DOI <https://doi.org/10.1016/j.actamat.2021.116937>. URL <https://www.sciencedirect.com/science/article/pii/S1359645421003177>.
- [18] Bouchard, P. J., Withers, P. J., McDonald, S. A. and Heenan, R. K. “Quantification of creep cavitation dam-

- age around a crack in a stainless steel pressure vessel." *Acta Materialia* Vol. 52 (2004): pp. 23–34. DOI [10.1016/J.ACTAMAT.2003.08.022](https://doi.org/10.1016/J.ACTAMAT.2003.08.022).
- [19] Turski, M., Bouchard, P. J., Steuwer, A. and Withers, P. J. "Residual stress driven creep cracking in AISI Type 316 stainless steel." *Acta Materialia* Vol. 56 (2008): pp. 3598–3612. DOI [10.1016/J.ACTAMAT.2008.03.045](https://doi.org/10.1016/J.ACTAMAT.2008.03.045).
- [20] Coules, H. E., Nneji, S. O., James, J. A., Kabra, S., Hu, J. N. and Wang, Y. "Full-tensor Measurement of Multiaxial Creep Stress Relaxation in Type 316H Stainless Steel." *Experimental Mechanics* Vol. 62 (2022): pp. 19–33. DOI [10.1007/S11340-021-00755-0/FIGURES/13](https://doi.org/10.1007/S11340-021-00755-0/FIGURES/13). URL <https://link.springer.com/article/10.1007/s11340-021-00755-0>.
- [21] Hossain, S., Truman, C. E. and Smith, D. J. "Generation of residual stress and plastic strain in a fracture mechanics specimen to study the formation of creep damage in type 316 stainless steel." *Fatigue & Fracture of Engineering Materials & Structures* Vol. 34 (2011): pp. 654–666. DOI [10.1111/J.1460-2695.2011.01557.X](https://doi.org/10.1111/J.1460-2695.2011.01557.X). URL <https://onlinelibrary.wiley.com/doi/full/10.1111/j.1460-2695.2011.01557.x><https://onlinelibrary.wiley.com/doi/abs/10.1111/j.1460-2695.2011.01557.x><https://onlinelibrary.wiley.com/doi/10.1111/j.1460-2695.2011.01557.x>.
- [22] Brown, D. W., Bernardin, J. D., Carpenter, J. S., Clausen, B., Spernjak, D. and Thompson, J. M. "Neutron diffraction measurements of residual stress in additively manufactured stainless steel." *Materials Science and Engineering: A* Vol. 678 (2016): pp. 291–298. DOI [10.1016/J.MSEA.2016.09.086](https://doi.org/10.1016/J.MSEA.2016.09.086).
- [23] Hossain, S., Truman, C. E., Smith, D. J., Peng, R. L. and Stuhr, U. "A study of the generation and creep relaxation of triaxial residual stresses in stainless steel." *International Journal of Solids and Structures* Vol. 44 (2007): pp. 3004–3020. DOI [10.1016/J.IJSOLSTR.2006.09.001](https://doi.org/10.1016/J.IJSOLSTR.2006.09.001).
- [24] Chen, B., Flewitt, P. E.J. and Smith, D. J. "Microstructural sensitivity of 316H austenitic stainless steel: Residual stress relaxation and grain boundary fracture." *Materials Science and Engineering: A* Vol. 527 (2010): pp. 7387–7399. DOI [10.1016/J.MSEA.2010.08.010](https://doi.org/10.1016/J.MSEA.2010.08.010).
- [25] Mirzaee-Sisan, A., Smith, D. J. and Truman, C. E. "Characterizing residual stresses in rectangular beam specimens following thermomechanical loading." <http://dx.doi.org/10.1243/03093247JSA215> Vol. 42 (2007): pp. 79–93. DOI [10.1243/03093247JSA215](https://doi.org/10.1243/03093247JSA215). URL https://journals.sagepub.com/doi/abs/10.1243/03093247jsa215?casa_token=0PYaHKf9BzEAAAAA%3AkImvHXHYqWDdh0MyJZPrIGDMMf9es9jkYiXii6hcrKXI_JcPkI1CHY0PJf0iwbjw6lS293Ixpqw8sQg.
- [26] Grilli, N., Cocks, A.C.F. and Tarleton, E. "Crystal plasticity finite element simulations of cast α -uranium." Onate, E, Owen, DRJ, Peric, D and Chiumenti, M (eds.). *Computational plasticity XV: fundamentals and applications*. Proceedings paper. 2019. 15th International Conference on Computational Plasticity - Fundamentals and Applications (COMPLAS), Barcelona, Spain, Sep 03-05, 2019.
- [27] Kapoor, Kartik, Ravi, Priya, Noraas, Ryan, Park, Jun-Sang, Venkatesh, Vasishth and Sangid, Michael D. "Modelling Ti-6Al-4V using crystal plasticity, calibrated with multi-scale experiments, to understand the effect of the orientation and morphology of the α and β phases on time dependent cyclic loading." *Journal of the Mechanics and Physics of Solids* Vol. 146 (2021): p. 104192. DOI <https://doi.org/10.1016/j.jmps.2020.104192>. URL <https://www.sciencedirect.com/science/article/pii/S0022509620304178>.
- [28] Grilli, Nicolò, Tarleton, Edmund, Edmondson, Philip D., Gussev, Maxim N. and Cocks, Alan C. F. "In situ measurement and modelling of the growth and length scale of twins in α -uranium." *Phys. Rev. Mater.* Vol. 4 (2020): p. 043605. DOI [10.1103/PhysRevMaterials.4.043605](https://doi.org/10.1103/PhysRevMaterials.4.043605). URL <https://link.aps.org/doi/10.1103/PhysRevMaterials.4.043605>.
- [29] Kapoor, Kartik. "Experimentally Validated Crystal Plasticity Modeling of Titanium Alloys at Multiple Length-Scales Based on Material Characterization, Accounting for Residual Stresses." Ph.D. Thesis, Purdue University. 2019. URL <https://www.proquest.com/docview/2827704223?pq-origsite=gscholar&fromopenview=true&sourcetype=Dissertations%20&%20Theses>.
- [30] Hossain, S., Truman, C.E., Smith, D.J. and Daymond, M.R. "Application of quenching to create highly triaxial residual stresses in type 316H stainless steels." *International Journal of Mechanical Sciences* Vol. 48 No. 3 (2006): pp. 235–243. DOI <https://doi.org/10.1016/j.ijmecsci.2005.11.002>. URL <https://www.sciencedirect.com/science/article/pii/S0020740305002675>.
- [31] Irastorza-Landa, A., Van Swygenhoven, H., Van Pelegem, S., Grilli, N., Bollhalder, A., Brandstetter, S. and Grolimund, D. "Following dislocation patterning during fatigue." *Acta Materialia* Vol. 112 (2016): pp. 184–193. DOI <https://doi.org/10.1016/j.actamat.2016.04.011>. URL <https://www.sciencedirect.com/science/article/pii/S1359645416302671>.
- [32] Ramadhan, Ranggi S., Glaser, Daniel, Soyama, Hitoshi, Kockelmann, Winfried, Shinohara, Takenao, Pirling, Thilo, Fitzpatrick, Michael E. and Tremsin, Anton S. "Mechanical surface treatment studies by Bragg edge neutron imaging." *Acta Materialia* Vol. 239 (2022): p. 118259. DOI <https://doi.org/10.1016/j.actamat.2022.118259>. URL <https://www.sciencedirect.com/science/article/pii/S1359645422006395>.
- [33] Zheng, Gang, Hossain, Sayeed, Kingston, Ed, Truman, Christopher E. and Smith, David J. "An optimisation study of the modified deep-hole drilling technique using finite element analyses applied to a stainless steel ring welded circular disc." *International Journal of Solids and Structures* Vol. 118-119 (2017): pp. 146–166. DOI <https://doi.org/10.1016/j.ijsolstr.2017.04.008>. URL <https://www.sciencedirect.com/science/article/pii/S0020768317301592>.
- [34] Baldi, A. "Residual Stress Measurement Using Hole Drilling and Integrated Digital Image Correlation Techniques." *Experimental Mechanics* Vol. 54 No. 3 (2014): pp. 379–391. DOI [10.1007/s11340-013](https://doi.org/10.1007/s11340-013-013).

- 9814-6. URL <https://link.springer.com/article/10.1007/s11340-013-9814-6>.
- [35] Grilli, Nicolò, Earp, Philip, Cocks, Alan C.F., Marrow, James and Tarleton, Edmund. “Characterisation of slip and twin activity using digital image correlation and crystal plasticity finite element simulation: Application to orthorhombic α -uranium.” *Journal of the Mechanics and Physics of Solids* Vol. 135 (2020): p. 103800. DOI <https://doi.org/10.1016/j.jmps.2019.103800>. URL <https://www.sciencedirect.com/science/article/pii/S0022509619306696>.
- [36] Behrens, B. -A, Brunotte, K., Wester, H. and Kock, C. “Targeted adjustment of residual stresses in hot-formed components by means of process design based on finite element simulation.” *Archive of Applied Mechanics* Vol. 91 (2021): pp. 3579–3602. DOI [10.1007/S00419-021-01928-Y/FIGURES/16](https://doi.org/10.1007/S00419-021-01928-Y/FIGURES/16). URL <https://link.springer.com/article/10.1007/s00419-021-01928-y>.
- [37] Perl, M., Kamal, S. M. and Mulera, Solomon. “The Use of an Equivalent Temperature Field to Emulate an Induced Residual Stress Field in a Rotating Disk Due to Full or Partial Rotational Autofrettage.” *Journal of Pressure Vessel Technology, Transactions of the ASME* Vol. 144 (2022). DOI [10.1115/1.4053880/1136719](https://doi.org/10.1115/1.4053880/1136719). URL <https://dx.doi.org/10.1115/1.4053880>.
- [38] Kapadia, P., Zhou, H., Davies, C. M., Wimpory, R. C. and Nikbin, K. M. “Simulating Residual Stresses Using a Modified Wedge-Loaded Compact Tension Specimen.” *American Society of Mechanical Engineers, Pressure Vessels and Piping Division (Publication) PVP* Vol. 6 A (2014). DOI [10.1115/PVP2013-97942](https://doi.org/10.1115/PVP2013-97942). URL <https://dx.doi.org/10.1115/PVP2013-97942>.
- [39] Xiong, Yi, Grilli, Nicolò, Karamched, Phani S., Li, Bo-Shiuan, Tarleton, Edmund and Wilkinson, Angus J. “Cold dwell behaviour of Ti₆Al alloy: Understanding load shedding using digital image correlation and dislocation based crystal plasticity simulations.” *Journal of Materials Science & Technology* Vol. 128 (2022): pp. 254–272. DOI <https://doi.org/10.1016/j.jmst.2022.05.034>. URL <https://www.sciencedirect.com/science/article/pii/S1005030222004881>.
- [40] Xiong, Yi, Grilli, Nicolò, Karamched, Phani S., Li, Bo-Shiuan, Tarleton, Edmund and Wilkinson, Angus J. “Cold dwell behaviour of Ti₆Al alloy: Understanding load shedding using digital image correlation and crystal plasticity simulations.” (2021). URL [2106.12227](https://doi.org/10.1115/PVP2013-97942).
- [41] Smith, M.C., Bouchard, P.J., Turski, M., Edwards, L. and Dennis, R.J. “Accurate prediction of residual stress in stainless steel welds.” *Computational Materials Science* Vol. 54 (2012): pp. 312–328. DOI <https://doi.org/10.1016/j.commatsci.2011.10.024>. URL <https://www.sciencedirect.com/science/article/pii/S0927025611005957>.
- [42] Muránsky, O., Hamelin, C.J., Smith, M.C., Bendeich, P.J. and Edwards, L. “The effect of plasticity theory on predicted residual stress fields in numerical weld analyses.” *Computational Materials Science* Vol. 54 (2012): pp. 125–134. DOI <https://doi.org/10.1016/j.commatsci.2011.10.026>. URL <https://www.sciencedirect.com/science/article/pii/S0927025611005970>.
- [43] Muránsky, O., Smith, M.C., Bendeich, P.J., Holden, T.M., Luzin, V., Martins, R.V. and Edwards, L. “Comprehensive numerical analysis of a three-pass bead-in-slot weld and its critical validation using neutron and synchrotron diffraction residual stress measurements.” *International Journal of Solids and Structures* Vol. 49 No. 9 (2012): pp. 1045–1062. DOI <https://doi.org/10.1016/j.ijsolstr.2011.07.006>. URL <https://www.sciencedirect.com/science/article/pii/S0020768311002538>.
- [44] Hamelin, Cory J., Muránsky, Ondrej, Smith, Michael C., Holden, Thomas M., Luzin, Vladimir, Bendeich, Philip J. and Edwards, Lyndon. “Validation of a numerical model used to predict phase distribution and residual stress in ferritic steel weldments.” *Acta Materialia* Vol. 75 (2014): pp. 1–19. DOI <https://doi.org/10.1016/j.actamat.2014.04.045>. URL <https://www.sciencedirect.com/science/article/pii/S1359645414002961>.
- [45] Lebensohn, R.A. and Tomé, C.N. “A self-consistent anisotropic approach for the simulation of plastic deformation and texture development of polycrystals: Application to zirconium alloys.” *Acta Metallurgica et Materialia* Vol. 41 No. 9 (1993): pp. 2611–2624. DOI [https://doi.org/10.1016/0956-7151\(93\)90130-K](https://doi.org/10.1016/0956-7151(93)90130-K). URL <https://www.sciencedirect.com/science/article/pii/095671519390130K>.
- [46] Roters, F., Diehl, M., Shanthraj, P., Eisenlohr, P., Reuber, C., Wong, S.L., Maiti, T., Ebrahimi, A., Hochrainer, T., Fabritius, H.-O., Nikolov, S., Friák, M., Fujita, N., Grilli, N., Janssens, K.G.F., Jia, N., Kok, P.J.J., Ma, D., Meier, F., Werner, E., Stricker, M., Weygand, D. and Raabe, D. “DAMASK – The Düsseldorf Advanced Material Simulation Kit for modeling multi-physics crystal plasticity, thermal, and damage phenomena from the single crystal up to the component scale.” *Computational Materials Science* Vol. 158 (2019): pp. 420–478. DOI <https://doi.org/10.1016/j.commatsci.2018.04.030>. URL <https://www.sciencedirect.com/science/article/pii/S0927025618302714>.
- [47] Lindroos, Matti, Pinomaa, Tuuli, Ammar, Kais, Laukkanen, Anssi, Provatas, Nikolas and Forest, Samuel. “Dislocation density in cellular rapid solidification using phase field modeling and crystal plasticity.” *International Journal of Plasticity* Vol. 148 (2022): p. 103139. DOI [10.1016/j.ijplas.2021.103139](https://doi.org/10.1016/j.ijplas.2021.103139).
- [48] Grilli, Nicolò, Hu, Daijun, Yushu, Dewen, Chen, Fan and Yan, Wentao. “Crystal plasticity model of residual stress in additive manufacturing using the element elimination and reactivation method.” *Computational Mechanics* Vol. 69 (2022): pp. 825–845. DOI [10.1007/S00466-021-02116-Z/FIGURES/17](https://doi.org/10.1007/S00466-021-02116-Z/FIGURES/17). URL <https://link.springer.com/article/10.1007/s00466-021-02116-z>.
- [49] Yan, Wentao, Ge, Wenjun, Qian, Ya, Lin, Stephen, Zhou, Bin, Liu, Wing Kam, Lin, Feng and Wagner,

- Gregory J. "Multi-physics modeling of single/multiple-track defect mechanisms in electron beam selective melting." *Acta Materialia* Vol. 134 (2017): pp. 324–333. DOI <https://doi.org/10.1016/j.actamat.2017.05.061>. URL <https://www.sciencedirect.com/science/article/pii/S1359645417304500>.
- [50] Wang, Lu, Wang, Shuhao, Zhang, Yanming and Yan, Wentao. "Multi-phase flow simulation of powder streaming in laser-based directed energy deposition." *International Journal of Heat and Mass Transfer* Vol. 212 (2023): p. 124240. DOI <https://doi.org/10.1016/j.ijheatmasstransfer.2023.124240>. URL <https://www.sciencedirect.com/science/article/pii/S0017931023003927>.
- [51] Hu, Jianan, Green, Graham, Hogg, Simon, Higginson, Rebecca and Cocks, Alan. "Effect of microstructure evolution on the creep properties of a polycrystalline 316H austenitic stainless steel." *Materials Science and Engineering: A* Vol. 772 (2020): p. 138787. DOI [10.1016/J.MSEA.2019.138787](https://doi.org/10.1016/J.MSEA.2019.138787).
- [52] Mamun, Abdullah Al, Simpson, Chris, Erinoshio, Tomiwa, Agius, Dylan, Reinhard, Christina, Mostafavi, Mahmoud and Knowles, David. "Effect of Plasticity on Creep Deformation in Type 316H Stainless Steel." *American Society of Mechanical Engineers, Pressure Vessels and Piping Division (Publication) PVP* Vol. 6A-2019 (2019). DOI [10.1115/PVP2019-93587](https://doi.org/10.1115/PVP2019-93587). URL <https://dx.doi.org/10.1115/PVP2019-93587>.
- [53] Petkov, Markian P., Hu, Jianan and Cocks, Alan C.F. "Self-consistent modelling of cyclic loading and relaxation in austenitic 316H stainless steel." *Philosophical Magazine* Vol. 99 (2019): pp. 789–834. DOI [10.1080/14786435.2018.1556407](https://doi.org/10.1080/14786435.2018.1556407). URL <https://www.tandfonline.com/doi/abs/10.1080/14786435.2018.1556407>.
- [54] Horton, Edward W., Spadotto, Julio C., Smith, Albert D., Donoghue, Jack M., Knowles, David, Connolly, Brian, Pickering, Ed J. and Mostafavi, Mahmoud. "Validation of Deformation in Crystal Plasticity When Modelling 316H Stainless Steel for Use in Pressure Vessels." *American Society of Mechanical Engineers, Pressure Vessels and Piping Division (Publication) PVP* Vol. 5 (2023). DOI [10.1115/PVP2023-101501](https://doi.org/10.1115/PVP2023-101501). URL <https://dx.doi.org/10.1115/PVP2023-101501>.
- [55] Mokhtarishirazabad, Mehdi, McMillan, Martin, Vijayanand, V. D., Simpson, Chris, Agius, Dylan, Truman, Christopher, Knowles, David and Mostafavi, Mahmoud. "Predicting residual stress in a 316L electron beam weld joint incorporating plastic properties derived from a crystal plasticity finite element model." *International Journal of Pressure Vessels and Piping* Vol. 201 (2023): p. 104868. DOI [10.1016/J.IJPVP.2022.104868](https://doi.org/10.1016/J.IJPVP.2022.104868).
- [56] Irastorza-Landa, A., Grilli, N. and Van Swygenhoven, H. "Laue micro-diffraction and crystal plasticity finite element simulations to reveal a vein structure in fatigued Cu." *Journal of the Mechanics and Physics of Solids* Vol. 104 (2017): pp. 157–171. DOI <https://doi.org/10.1016/j.jmps.2017.04.010>. URL <https://www.sciencedirect.com/science/article/pii/S0022509616304781>.
- [57] Flint, TF, Sun, YL, Xiong, Qingrong, Smith, MC and Francis, JA. "Phase-field simulation of grain boundary evolution in microstructures containing second-phase particles with heterogeneous thermal properties." *Scientific Reports* Vol. 9 No. 1 (2019): p. 18426.
- [58] Kristensen, Philip K., Niordson, Christian F. and Martínez-Pañeda, Emilio. "An assessment of phase field fracture: crack initiation and growth." *Philosophical Transactions of the Royal Society A: Mathematical, Physical and Engineering Sciences* Vol. 379 No. 2203 (2021): p. 20210021. DOI [10.1098/rsta.2021.0021](https://doi.org/10.1098/rsta.2021.0021). URL <https://royalsocietypublishing.org/doi/pdf/10.1098/rsta.2021.0021>, URL <https://royalsocietypublishing.org/doi/abs/10.1098/rsta.2021.0021>.
- [59] Kumar, Aditya, Bourdin, Blaise, Francfort, Gilles A. and Lopez-Pamies, Oscar. "Revisiting nucleation in the phase-field approach to brittle fracture." *Journal of the Mechanics and Physics of Solids* Vol. 142 (2020): p. 104027. DOI <https://doi.org/10.1016/j.jmps.2020.104027>. URL <https://www.sciencedirect.com/science/article/pii/S0022509620302623>.
- [60] Dittmann, M., Aldakheel, F., Schulte, J., Schmidt, F., Krüger, M., Wriggers, P. and Hesch, C. "Phase-field modeling of porous-ductile fracture in non-linear thermo-elasto-plastic solids." *Computer Methods in Applied Mechanics and Engineering* Vol. 361 (2020): p. 112730. DOI <https://doi.org/10.1016/j.cma.2019.112730>. URL <https://www.sciencedirect.com/science/article/pii/S0045782519306206>.
- [61] Salvini, Michael, Grilli, Nicolò, Demir, Eralp, He, Siqi, Martin, Tomas, Flewitt, Peter, Mostafavi, Mahmoud, Truman, Christopher and Knowles, David. "Effect of grain boundary misorientation and carbide precipitation on damage initiation: A coupled crystal plasticity and phase field damage study." *International Journal of Plasticity* Vol. 172 (2024): p. 103854. DOI <https://doi.org/10.1016/j.ijplas.2023.103854>. URL <https://www.sciencedirect.com/science/article/pii/S0749641923003388>.
- [62] Abrivard, G., Busso, E.P., Forest, S. and Appolaire, B. "Phase field modelling of grain boundary motion driven by curvature and stored energy gradients. Part I: theory and numerical implementation." *Philosophical Magazine* Vol. 92 No. 28-30 (2012): pp. 3618–3642.
- [63] Ask, Anna, Forest, Samuel, Appolaire, Benoit and Ammar, Kais. "A Cosserat–phase-field theory of crystal plasticity and grain boundary migration at finite deformation." *Continuum Mechanics and Thermodynamics* Vol. 31 No. 4 (2019): pp. 1109–1141.
- [64] Prahs, Andreas, Schöller, Lukas, Schwab, Felix K, Schneider, Daniel, Böhlke, Thomas and Nestler, Britta. "A multiphase-field approach to small strain crystal plasticity accounting for balance equations on singular surfaces." *Computational Mechanics* (2023): pp. 1–22.

- [65] Ali, Muhammad Adil, Shchyglo, Oleg, Stricker, Markus and Steinbach, Ingo. "Coherency loss marking the onset of degradation in high temperature creep of superalloys: Phase-field simulation coupled to strain gradient crystal plasticity." *Computational Materials Science* Vol. 220 (2023): p. 112069.
- [66] Koslowski, Marisol, Grilli, Nicolo, Tanasoiu, Bogdan and Duarte Cordon, Camilo. "Dynamic failure of high energy materials under compression and periodic excitation." *APS Shock Compression of Condensed Matter Meeting Abstracts*: p. V5.005. 2017.
- [67] Grilli, Nicolò and Koslowski, Marisol. "The effect of crystal orientation on shock loading of single crystal energetic materials." *Computational Materials Science* Vol. 155 (2018): pp. 235–245. DOI <https://doi.org/10.1016/j.commatsci.2018.08.059>. URL <https://www.sciencedirect.com/science/article/pii/S0927025618305883>.
- [68] Duarte, Camilo, Koslowski, Marisol and Grilli, Nicolo. "Modeling the effect of plasticity and damage in β -HMX single crystals under shock loading." *21st Biennial Conference of the APS Topical Group on Shock Compression of Condensed Matter*. 2019.
- [69] Miehe, C., Welschinger, F. and Hofacker, M. "Thermodynamically consistent phase-field models of fracture: Variational principles and multi-field FE implementations." *International Journal for Numerical Methods in Engineering* Vol. 83 No. 10 (2010): pp. 1273–1311. DOI <https://doi.org/10.1002/nme.2861>. URL <https://onlinelibrary.wiley.com/doi/pdf/10.1002/nme.2861>, URL <https://onlinelibrary.wiley.com/doi/abs/10.1002/nme.2861>.
- [70] Permann, Cody J., Gaston, Derek R., Andra, David, Carlsen, Robert W., Kong, Fande, Lindsay, Alexander D., Miller, Jason M., Peterson, John W., Slaughter, Andrew E., Stogner, Roy H. and Martineau, Richard C. "MOOSE: Enabling massively parallel multiphysics simulation." *SoftwareX* Vol. 11 (2020): p. 100430. DOI <https://doi.org/10.1016/j.softx.2020.100430>. URL <https://www.sciencedirect.com/science/article/pii/S2352711019302973>.
- [71] Kalidindi, S.R., Bronkhorst, C.A. and Anand, L. "Crystallographic texture evolution in bulk deformation processing of FCC metals." *Journal of the Mechanics and Physics of Solids* Vol. 40 No. 3 (1992): pp. 537–569. DOI [https://doi.org/10.1016/0022-5096\(92\)80003-9](https://doi.org/10.1016/0022-5096(92)80003-9). URL <https://www.sciencedirect.com/science/article/pii/0022509692800039>.
- [72] Rice, J.R. "Inelastic constitutive relations for solids: An internal-variable theory and its application to metal plasticity." *Journal of the Mechanics and Physics of Solids* Vol. 19 No. 6 (1971): pp. 433–455. DOI [https://doi.org/10.1016/0022-5096\(71\)90010-X](https://doi.org/10.1016/0022-5096(71)90010-X). URL <https://www.sciencedirect.com/science/article/pii/002250967190010X>.
- [73] Staroselsky, Alexander and Cassenti, Brice N. "Creep, plasticity, and fatigue of single crystal superalloy." *International Journal of Solids and Structures* Vol. 48 No. 13 (2011): pp. 2060–2075. DOI <https://doi.org/10.1016/j.ijsolstr.2011.03.011>. URL <https://www.sciencedirect.com/science/article/pii/S0020768311001132>.
- [74] Skamniotis, Christos, Grilli, Nicolò and Cocks, Alan C.F. "Crystal plasticity analysis of fatigue-creep behavior at cooling holes in single crystal Nickel based gas turbine blade components." *International Journal of Plasticity* Vol. 166 (2023): p. 103589. DOI <https://doi.org/10.1016/j.ijplas.2023.103589>. URL <https://www.sciencedirect.com/science/article/pii/S074964192300075X>.
- [75] Bayley, C.J., Brekelmans, W.A.M. and Geers, M.G.D. "A comparison of dislocation induced back stress formulations in strain gradient crystal plasticity." *International Journal of Solids and Structures* Vol. 43 No. 24 (2006): pp. 7268–7286. DOI <https://doi.org/10.1016/j.ijsolstr.2006.05.011>. URL <https://www.sciencedirect.com/science/article/pii/S0020768306001697>. Size-dependent Mechanics of Materials.
- [76] Franciosi, P. and Zaoui, A. "Multislip in f.c.c. crystals a theoretical approach compared with experimental data." *Acta Metallurgica* Vol. 30 No. 8 (1982): pp. 1627–1637. DOI [https://doi.org/10.1016/0001-6160\(82\)90184-5](https://doi.org/10.1016/0001-6160(82)90184-5). URL <https://www.sciencedirect.com/science/article/pii/0001616082901845>.
- [77] Grilli, Nicolò. "Physics-based constitutive modelling for crystal plasticity finite element computation of cyclic plasticity in fatigue." Ph.D. Thesis, École Polytechnique Fédérale de Lausanne. 2016. DOI <10.5075/epfl-thesis-7251>. URL <https://infoscience.epfl.ch/record/223625>.
- [78] Franciosi, P., Berveiller, M. and Zaoui, A. "Latent hardening in copper and aluminium single crystals." *Acta Metallurgica* Vol. 28 No. 3 (1980): pp. 273–283. DOI [https://doi.org/10.1016/0001-6160\(80\)90162-5](https://doi.org/10.1016/0001-6160(80)90162-5). URL <https://www.sciencedirect.com/science/article/pii/0001616080901625>.
- [79] Grilli, N., Janssens, K.G.F., Nellessen, J., Sandlöbes, S. and Raabe, D. "Multiple slip dislocation patterning in a dislocation-based crystal plasticity finite element method." *International Journal of Plasticity* Vol. 100 (2018): pp. 104–121. DOI <https://doi.org/10.1016/j.ijplas.2017.09.015>. URL <https://www.sciencedirect.com/science/article/pii/S0749641917305570>.
- [80] Grilli, Nicolò, Janssens, Koenraad G.F. and Van Swygenhoven, Helena. "Crystal plasticity finite element modelling of low cycle fatigue in fcc metals." *Journal of the Mechanics and Physics of Solids* Vol. 84 (2015): pp. 424–435. DOI <https://doi.org/10.1016/j.jmps.2015.08.007>. URL <https://www.sciencedirect.com/science/article/pii/S0022509615300727>.
- [81] Hu, Daijun, Grilli, Nicolò and Yan, Wentao. "Dislocation structures formation induced by thermal stress in additive manufacturing: Multiscale crystal plastic-

- ity modeling of dislocation transport.” *Journal of the Mechanics and Physics of Solids* Vol. 173 (2023): p. 105235. DOI <https://doi.org/10.1016/j.jmps.2023.105235>. URL <https://www.sciencedirect.com/science/article/pii/S002250962300039X>.
- [82] Catalao, S., Feaugas, X., Pilvin, Ph. and Cabrillat, M.-Th. “Dipole heights in cyclically deformed polycrystalline AISI 316L stainless steel.” *Materials Science and Engineering: A* Vol. 400-401 (2005): pp. 349–352. DOI <https://doi.org/10.1016/j.msea.2005.03.094>. URL <https://www.sciencedirect.com/science/article/pii/S0921509305003242>. Dislocations 2004.
- [83] Ashby, MF. “The deformation of plastically non-homogeneous materials.” *The Philosophical Magazine: A Journal of Theoretical Experimental and Applied Physics* Vol. 21 No. 170 (1970): pp. 399–424. DOI [10.1080/14786437008238426](https://doi.org/10.1080/14786437008238426). URL <https://doi.org/10.1080/14786437008238426>.
- [84] Yalçinkaya, T., Tandoğan, İ.T. and Özdemir, İ. “Void growth based inter-granular ductile fracture in strain gradient polycrystalline plasticity.” *International Journal of Plasticity* Vol. 147 (2021): p. 103123. DOI <https://doi.org/10.1016/j.ijplas.2021.103123>. URL <https://www.sciencedirect.com/science/article/pii/S0749641921001911>.
- [85] Hu, Daijun, Guo, Zixu, Grilli, Nicolò, Tay, Aloysius, Lu, Zhen and Yan, Wentao. “Understanding the strain localization in additively manufactured materials: micro-scale tensile tests and crystal plasticity modeling.” (*submitted manuscript*) (2024).
- [86] Ortiz, M. and Pandolfi, A. “Finite-deformation irreversible cohesive elements for three-dimensional crack-propagation analysis.” *International Journal for Numerical Methods in Engineering* Vol. 44 No. 9 (1999): pp. 1267–1282. DOI [https://doi.org/10.1002/\(SICI\)1097-0207\(19990330\)44:9<1267::AID-NME486>3.0.CO;2-7](https://doi.org/10.1002/(SICI)1097-0207(19990330)44:9<1267::AID-NME486>3.0.CO;2-7). URL [https://onlinelibrary.wiley.com/doi/10.1002/\(SICI\)1097-0207\(19990330\)44:9%3C1267::AID-NME486%3E3.0.CO;2-7](https://onlinelibrary.wiley.com/doi/10.1002/(SICI)1097-0207(19990330)44:9%3C1267::AID-NME486%3E3.0.CO;2-7).
- [87] Grilli, Nicolò, Tarleton, Edmund and Cocks, Alan C.F. “Neper2CAE and PyCiGen: Scripts to generate polycrystals and interface elements in Abaqus.” *SoftwareX* Vol. 13 (2021): p. 100651. DOI <https://doi.org/10.1016/j.softx.2020.100651>. URL <https://www.sciencedirect.com/science/article/pii/S2352711020303642>.
- [88] Grilli, Nicolò, Tarleton, Edmund and Cocks, Alan C. F. “Coupling a discrete twin model with cohesive elements to understand twin-induced fracture.” *International Journal of Fracture* Vol. 227 No. 2 (2021): pp. 173–192. DOI [10.1007/s10704-020-00504-9](https://doi.org/10.1007/s10704-020-00504-9). URL <https://link.springer.com/article/10.1007/s10704-020-00504-9#citeas>.
- [89] Grilli, Nicolò, Cocks, Alan C. F. and Tarleton, Edmund. “Modelling the nucleation and propagation of cracks at twin boundaries.” *International Journal of Fracture* Vol. 233 No. 1 (2022): pp. 17–38. DOI [10.1007/s10704-021-00606-y](https://doi.org/10.1007/s10704-021-00606-y). URL <https://link.springer.com/article/10.1007/s10704-021-00606-y#citeas>.
- [90] Grilli, Nicolò and Koslowski, Marisol. “The effect of crystal anisotropy and plastic response on the dynamic fracture of energetic materials.” *Journal of Applied Physics* Vol. 126 No. 15 (2019): p. 155101. DOI [10.1063/1.5109761](https://doi.org/10.1063/1.5109761). URL <https://doi.org/10.1063/1.5109761>, URL <https://doi.org/10.1063/1.5109761>.
- [91] Grilli, Nicolo, Dandekar, Akshay and Koslowski, Marisol. “Coupling crystal plasticity and phase-field damage to simulate β -HMX-based polymer-bonded explosive under shock load.” *APS Shock Compression of Condensed Matter Meeting Abstracts*: p. Z4.002. 2017. URL <https://ui.adsabs.harvard.edu/abs/2017APS..SHK.Z4002G/abstract>.
- [92] Grilli, Nicolò, Duarte, Camilo A. and Koslowski, Marisol. “Dynamic fracture and hot-spot modeling in energetic composites.” *Journal of Applied Physics* Vol. 123 No. 6 (2018): p. 065101. DOI [10.1063/1.5009297](https://doi.org/10.1063/1.5009297). URL <https://doi.org/10.1063/1.5009297>, URL <https://doi.org/10.1063/1.5009297>.
- [93] Duarte, Camilo A., Grilli, Nicolò and Koslowski, Marisol. “Effect of initial damage variability on hot-spot nucleation in energetic materials.” *Journal of Applied Physics* Vol. 124 No. 2 (2018): p. 025104. DOI [10.1063/1.5030656](https://doi.org/10.1063/1.5030656). URL <https://doi.org/10.1063/1.5030656>, URL <https://doi.org/10.1063/1.5030656>.
- [94] Sakano, Michael N., Hamed, Ahmed, Kober, Edward M., Grilli, Nicolo, Hamilton, Brenden W., Islam, Md Mahbubul, Koslowski, Marisol and Strachan, Alejandro. “Unsupervised Learning-Based Multiscale Model of Thermochemistry in 1,3,5-Trinitro-1,3,5-triazinane (RDX).” *The Journal of Physical Chemistry A* Vol. 124 No. 44 (2020): pp. 9141–9155. DOI [10.1021/acs.jpca.0c07320](https://doi.org/10.1021/acs.jpca.0c07320). URL <https://pubs.acs.org/doi/full/10.1021/acs.jpca.0c07320>.
- [95] Ziegler, Hans. “An Introduction to Thermomechanics.” Vol. 21 of *North-Holland Series in Applied Mathematics and Mechanics*. North-Holland (1983). DOI <https://doi.org/10.1016/B978-0-444-86503-8.50002-0>. URL <https://www.sciencedirect.com/science/article/pii/B9780444865038500020>.
- [96] Lee, E. H. “Elastic-Plastic Deformation at Finite Strains.” *Journal of Applied Mechanics* Vol. 36 No. 1 (1969): pp. 1–6. DOI [10.1115/1.3564580](https://doi.org/10.1115/1.3564580). URL https://asmedigitalcollection.asme.org/appliedmechanics/article-pdf/36/1/1/5449476/1_1.pdf, URL <https://doi.org/10.1115/1.3564580>.
- [97] Griffith, Alan Arnold and Taylor, Geoffrey Ingram. “VI. The phenomena of rupture and flow in solids.” *Philosophical Transactions of the Royal Society of London. Series A, Containing Papers of a Mathematical or Physical Character* Vol. 221 No. 582–593 (1921): pp. 163–198. DOI [10.1098/rsta.1921.0006](https://doi.org/10.1098/rsta.1921.0006). URL <https://royalsocietypublishing.org/doi/pdf/10.1098/rsta.1921.0006>, URL <https://royalsocietypublishing.org/doi/abs/10.1098/rsta.1921.0006>.

- [98] Hu, Daijun, Grilli, Nicolò, Wang, Lu, Yang, Min and Yan, Wentao. “Microscale residual stresses in additively manufactured stainless steel: Computational simulation.” *Journal of the Mechanics and Physics of Solids* Vol. 161 (2022): p. 104822. DOI <https://doi.org/10.1016/j.jmps.2022.104822>. URL <https://www.sciencedirect.com/science/article/pii/S0022509622000394>.
- [99] Flint, Thomas F., Robson, Joseph D., Parivendhan, Gowthaman and Cardiff, Philip. “laserbeamFoam: Laser ray-tracing and thermally induced state transition simulation toolkit.” *SoftwareX* Vol. 21 (2023): p. 101299. DOI <https://doi.org/10.1016/j.softx.2022.101299>. URL <https://www.sciencedirect.com/science/article/pii/S2352711022002175>.
- [100] Flint, Thomas F., Robson, Joseph D., Esmati, Parsa, Grilli, Nicolò, Parivendhan, Gowthaman and Cardiff, Philip. “Version 2.0 — LaserbeamFoam: Laser ray-tracing and thermally induced state transition simulation toolkit.” *SoftwareX* Vol. 25 (2024): p. 101612. DOI <https://doi.org/10.1016/j.softx.2023.101612>. URL <https://www.sciencedirect.com/science/article/pii/S2352711023003084>.
- [101] Yang, Min, Wang, Lu and Yan, Wentao. “Phase-field modeling of grain evolutions in additive manufacturing from nucleation, growth, to coarsening.” *Npj Computational Materials* Vol. 7 No. 1 (2021): p. 56.
- [102] Moelans, N., Blanpain, B. and Wollants, P. “Quantitative analysis of grain boundary properties in a generalized phase field model for grain growth in anisotropic systems.” *Phys. Rev. B* Vol. 78 (2008): p. 024113. DOI [10.1103/PhysRevB.78.024113](https://doi.org/10.1103/PhysRevB.78.024113). URL <https://link.aps.org/doi/10.1103/PhysRevB.78.024113>.
- [103] Friedli, Jonathan, Napoli, Paolo Di, Rappaz, Michel and Dantzig, Jonathan A. “Phase-field modeling of the dendrite orientation transition in Al-Zn alloys.” *IOP Conference Series: Materials Science and Engineering* Vol. 33 No. 1 (2012): p. 012111. DOI [10.1088/1757-899X/33/1/012111](https://doi.org/10.1088/1757-899X/33/1/012111). URL <https://dx.doi.org/10.1088/1757-899X/33/1/012111>.
- [104] Grilli, Nicolò, Cocks, Alan C.F. and Tarleton, Edmund. “A phase field model for the growth and characteristic thickness of deformation-induced twins.” *Journal of the Mechanics and Physics of Solids* Vol. 143 (2020): p. 104061. DOI <https://doi.org/10.1016/j.jmps.2020.104061>. URL <https://www.sciencedirect.com/science/article/pii/S0022509620302957>.
- [105] Zhang, Peilei, Jia, Zhiyuan, Yu, Zhishui, Shi, Haichuan, Li, Shaowei, Wu, Di, Yan, Hua, Ye, Xin, Chen, Jieshi, Wang, Fuxin and Tian, Yingtao. “A review on the effect of laser pulse shaping on the microstructure and hot cracking behavior in the welding of alloys.” *Optics & Laser Technology* Vol. 140 (2021): p. 107094. DOI <https://doi.org/10.1016/j.optlastec.2021.107094>. URL <https://www.sciencedirect.com/science/article/pii/S0030399221001821>.
- [106] Lemaitre, Jean and Chaboche, Jean-Louis. *Mechanics of Solid Materials*. Cambridge University Press (1990).
- [107] Yilbas, B. S. and Akhtar, Sohail. “Laser Welding of AISI 316 Steel: Microstructural and Stress Analysis.” *Journal of Manufacturing Science and Engineering* Vol. 135 No. 3 (2013): p. 031018. DOI [10.1115/1.4024155](https://doi.org/10.1115/1.4024155). URL https://asmedigitalcollection.asme.org/manufacturingscience/article-pdf/135/3/031018/6261249/manu_135_3_031018.pdf, URL <https://doi.org/10.1115/1.4024155>.
- [108] Petkov, Markian and Cocks, Alan. “Modelling microstructure evolution, creep deformation and damage in Type 316H stainless steel.” (2020) DOI [10.13039/100015567](https://doi.org/10.13039/100015567).
- [109] Shitong Wei, Dianbao Gao, Langlang Zhao and Lu, Shanning. “Microstructure evolution and mechanical properties of 316H weld metal during aging.” *Materials Science and Technology* Vol. 36 No. 7 (2020): pp. 793–804. DOI [10.1080/02670836.2020.1743597](https://doi.org/10.1080/02670836.2020.1743597). URL <https://doi.org/10.1080/02670836.2020.1743597>, URL <https://doi.org/10.1080/02670836.2020.1743597>.
- [110] Yoon, Ji-Hyun, Hong, Seokmin, Lee, Bong-Sang and Koo, Gyeong-Hoi. “Effects of Thermal Aging on Type 316H Stainless Steel for Reactor Vessel.” *Transactions of the Korean Nuclear Society Spring Meeting Jeju*.
- [111] Wilson-Heid, Alexander E., Wang, Zhuqing, McCornac, Brenna and Beese, Allison M. “Quantitative relationship between anisotropic strain to failure and grain morphology in additively manufactured Ti-6Al-4V.” *Materials Science and Engineering: A* Vol. 706 (2017): pp. 287–294. DOI <https://doi.org/10.1016/j.msea.2017.09.017>. URL <https://www.sciencedirect.com/science/article/pii/S0921509317311632>.
- [112] Del Guercio, G., McCartney, D.G., Aboulkhair, N.T., Robertson, S., MacLachlan, R., Tuck, C. and Simonelli, M. “Cracking behaviour of high-strength AA2024 aluminium alloy produced by Laser Powder Bed Fusion.” *Additive Manufacturing* Vol. 54 (2022): p. 102776. DOI <https://doi.org/10.1016/j.addma.2022.102776>. URL <https://www.sciencedirect.com/science/article/pii/S2214860422001804>.
- [113] Zhao, Lei, Qi, Xueyan, Xu, Lianyong, Han, Yongdian, Jing, Hongyang and Song, Kai. “Tensile mechanical properties, deformation mechanisms, fatigue behaviour and fatigue life of 316H austenitic stainless steel: Effects of grain size.” *Fatigue and Fracture of Engineering Materials and Structures* Vol. 44 (2021): pp. 533–550. DOI [10.1111/ffe.13378](https://doi.org/10.1111/ffe.13378).